PROCEEDINGS OF SCIENCE

Measurements of cosmic-ray proton and helium spectra from the ISS-CREAM experiment

G. H. Choi,[a,g,2,*] **E. S. Seo,**[b,c] **S. Aggarwal,**[b,c] **Y. Amare,**[b] **D. Angelaszek,**[b,c] **A. Bagga,**[a] **D. P. Bowman,**[b,c] **Y. C. Chen,**[b,c] **M. Copley,**[b] **L. Derome,**[d] **Z. M. Dorris,**[c] **L. Eraud,**[d] **J. H. Han,**[b] **A. Haque,**[b,c] **H. G. Huh,**[b] **S. Jeong,**[a] **S. C. Kang,**[e] **H. J. Kim,**[e] **K. C. Kim,**[b] **M. H. Kim,**[b] **J. Lee,**[e] **M. H. Lee,**[b] **M. J. Lee,**[a] **J. P. Lundquist,**[b] **L. Lutz,**[b] **S. Maricic,**[b,c] **A. Menchaca-Rocha,**[f] **O. Ofoha,**[b] **H. Park,**[e] **I. H. Park,**[a] **J. M. Park,**[e] **S. Pandey,**[b] **N. Picot-Clemente,**[b] **R. Scrandis,**[b] **R. P. Weinmann,**[b] **H. Wu,**[b] **J. Wu,**[b] **Y. S. Yoon**[b,c] **and H. G. Zhang**[b]

[a] *Dept. of Physics, Sungkyunkwan University, Suwon, South Korea*
[b] *Inst. for Phys. Sci. and Tech., University of Maryland, College Park, MD, USA*
[c] *Dept. of Physics, University of Maryland, College Park, MD, USA*
[d] *Univ. Grenoble Alpes, CNRS, LPSC-IN2P3, Grenoble, France*
[e] *Dept. of Physics, Kyungpook National University, Daegu, South Korea*
[f] *Instituto de Fisica, Universidad Nacional Autonoma de Mexico, Ciudad Universitaria, Mexico*
[g] *Korea Aerospace Research Institute, Daejeon, Republic of Korea*

E-mail: chgwangho@kari.re.kr

The Cosmic Ray Energetics And Mass for the International Space Station (ISS-CREAM) payload was developed to measure the elemental spectra for a charge range of Z = 1 to 26, with an energy range from $\sim 10^{12}$ to $\sim 10^{15}$eV. Launched in August 2017, the ISS-CREAM payload successfully collected data for 539 days until February 2019. The ISS-CREAM instrument consists of several particle detectors: a Silicon Charge Detector (SCD) for charge measurements and a calorimeter (CAL) with carbon targets for energy measurements. It also includes a top counting detector (TCD), a bottom counting detector (BCD), and a boronated scintillator detector (BSD) to help separate electrons from protons. For this analysis, SCD and CAL were used for the charge and energy measurement, respectively, while TCD/BCD and CAL were used for the trigger. The ISS-CREAM proton spectrum has been reported in the energy range of 1.6 − 655 TeV. This proton spectrum deviates from a single power-law, softening at ∼ 9 TeV. This study presents the preliminary helium spectrum from the ISS-CREAM experiment in the energy range of 6 TeV to ∼ 1.1 PeV.

39th International Cosmic Ray Conference (ICRC2025)
15–24 July 2025
Geneva, Switzerland

[1] Cosmic Ray Energetics And Mass for the International Space Station
[2] For the ISS-CREAM Collaboration
[*] Speaker

PoS(ICRC2025)028

1. Introduction

The ISS-CREAM payload was launched on August 14, 2017, aboard a SpaceX Falcon 9 rocket as part of NASA's 12th Commercial Resupply Services (CRS-12) mission from the Kennedy Space Center. It was subsequently delivered to the International Space Station (ISS) and installed on the Japanese Experiment Module Exposed Facility (JEM-EF) #2 on August 21, 2017 [1]. The purpose of the ISS-CREAM mission is to measure the high-energy cosmic rays from protons to iron nuclei, with an energy range of $\sim$ 1 TeV to $\sim$ 1 PeV. The payload includes several detectors: a Silicon Charge Detector (SCD), carbon targets (C-targets), a calorimeter (CAL), a Top Counting Detector (TCD), a Bottom Counting Detector (BCD), and a Boronated Scintillator Detector (BSD), as shown in Fig. 1.

The SCD, positioned at the top of the payload, comprises four layers dedicated to charge identification. Each layer has an area of 78.2×73.6 cm^2 and contains 2688 individually segmented silicon pixels. This configuration minimizes contamination from particles scattered back from the lower layers [2]. Located directly below the SCD are two graphite blocks that serve as carbon targets. These high-density targets promote hadronic interactions, initiating particle showers that are subsequently detected by the CAL [3]. The CAL itself is composed of 20 alternating layers of tungsten and scintillating fibers. It enables both energy measurements and directional reconstruction of incident particles based on the shower axis and spatial energy deposits [3].

The TCD and BCD, placed above and below the CAL, respectively, consist of segmented photodiode arrays. They provide measurements of shower development in both longitudinal and lateral directions, helping to distinguish electrons and protons [4]. These detectors also support a low-energy trigger system. At the bottom of the payload, the BSD helps electron/hadron separation by detecting delayed signals associated with thermal neutrons [5].

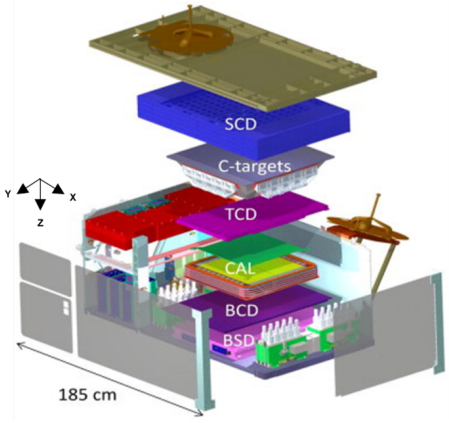

Figure 1: Exploded view of the ISS-CREAM instrument [1]

2. Data analysis

The ISS-CREAM instrument provides two physics triggers, generated by the CAL for the high-energy trigger (EHI) and TCD/BCD for the low-energy trigger (ELO). The EHI trigger has at least one ribbon in each of six consecutive CAL layers that measures energy deposits above a

typical threshold [6]. The ELO trigger condition requires that signals above specific thresholds are measured in at least one TCD and two BCD hits for the event to be accepted [4]. All events analyzed were selected based on the EHI or ELO trigger condition. Events corresponding to non-interacting particles or those initiating their first interaction below the top CAL layer, referred to as late interactions, were excluded from the dataset by using Equation (1) given below [7]. Such events can lead to significant errors in determining the deposited energy or the particle's charge due to the increased uncertainty in reconstructing the trajectory [7].

$$\log_{10}E_f(MeV) \geq -0.43 \cdot \log_{10}E_t(MeV) + 0.06, \tag{1}$$

where E_f is the deposited energy fraction from the top to fourth layers and E_t is the total deposited energy in CAL.

2.1 Trajectory reconstruction

The trajectory of an incident cosmic ray is determined by reconstructing its shower axis within the CAL. For the shower axis reconstruction, the ribbon with the highest energy deposit in each CAL layer is identified in both the XZ and YZ planes. For each projection, the layer with the maximum signal and its two nearest layers are selected to perform a linear fit. A chi-squared fit to a straight line through these three layers is used to define the preliminary shower axis [7]. Four combinations of three-layer subsets are tested for the initial fit: layers 1 and 2, 2 and 3, 3 and 1, and all three layers together. This preliminary axis is then extrapolated to the top and bottom layers of the CAL to establish an initial trajectory.

A selection criterion is applied next: for each layer, the ribbon with the highest signal is chosen if it lies within ±3 cm of the initial shower axis in both the XZ and YZ projections. Layers that satisfy this condition are used in a second linear fitting. Among these second fits, the one including the greatest number of layers is selected as the final shower axis. The sign of the slope from the final fit must match that of at least one of the four initial fits.

Figure 2 presents an example of shower axis reconstruction in the XZ plane. The red circles indicate the layers used in the final fit, shown as a red line. The ribbons with the largest signals in each layer are marked with × symbols.

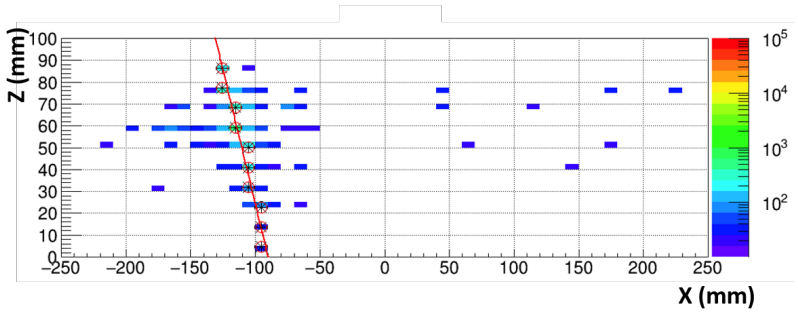

Figure 2: An illustration of the shower axis reconstruction in the CAL. The energy deposited in each ribbon is represented by color intensity. The ribbons with the highest energy deposits are marked with × symbols, and the circled crosses indicate the layers used in the final linear fit (red line) [7].

2.2 Charge measurement

To identify the incident particle, the reconstructed shower axis from the CAL is extrapolated to the SCD. An 11×11 pixel region centered on the extrapolated position is scanned to search for the incident particle. Within this area, the pixel with the maximum signal is selected as the hit candidate. The corresponding signal is then corrected for the particle's path length, which is determined from the reconstructed angle of incidence relative to the SCD plane [7].

Figure 3(a) presents the measured charge distributions of protons and helium nuclei observed in the first (black solid line), second (blue dashed line), and third layers (green dotted line) of the SCD. The event statistics in the third layer are reduced due to the loss of one quadrant after August 2018 [8]. To ensure sufficient statistics, only the top SCD layer was used in the charge analysis. The charge spectrum for protons and helium nuclei was fitted using a double Landau distribution, as shown in Fig. 3(b) [7]. The fitted charge peaks are located at $Z = 0.95$ for protons and $Z = 2.03$ for helium. The corresponding charge resolutions are 0.14 e and 0.15 e, respectively. The charge selection windows are defined as $0.7 < Z < 1.7$ for protons and $1.7 < Z < 2.7$ for helium.

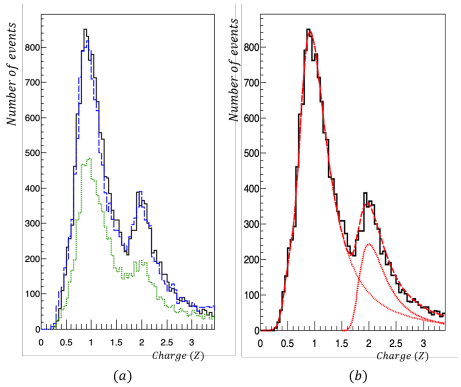

Figure 3: Measured charge distributions of proton and helium nuclei. (a) Charge spectra from individual SCD layers: black solid line (top layer), blue dashed line (second layer), and green dotted line (third layer). (b) Charge distribution from the top layer fitted with a double Landau distribution (red dashed line). The red dotted curves represent the individual contributions of protons and helium nuclei in the fit [7].

2.3 Spectral deconvolution

The total deposited energy for an incident particle is calculated by summing the deposited energy in all scintillating-fiber ribbons of the calorimeter(CAL). A detailed description of the CAL's energy calibration can be found in Zhang et al. 2021 [9] and references therein. In this analysis, events identified as protons and helium nuclei are counted in each reconstructed energy bin. The bin widths are chosen based on the statistical root-mean-square(rms) resolution of the CAL's energy response.

Due to finite energy resolution, events may be reconstructed in incorrect bins; therefore, corrections are applied to account for migrations between neighboring energy bins. To account for this bin migration, an unfolding procedure is applied. This involves solving a system of linear equations to relate the measured distribution to the true incident energy distribution. The transformation is expressed as follows [6]:

$$N_{\mathrm{inc},i} = \sum_j P_{i,j}\, N_{\mathrm{dep},j}, \tag{2}$$

where $N_{\mathrm{dep},j}$ represents the number of events observed in deposited energy bin j, and $N_{\mathrm{inc},i}$ is the inferred number of events in incident energy bin i. The matrix element $P_{i,j}$ denotes the probability that an event originating in incident energy bin i is reconstructed in deposited energy bin j. This response matrix is derived from Monte Carlo(MC) simulations conducted separately for proton and helium events.

2.4 Absolute flux

The absolute flux, F, is calculated by correcting the measured cosmic-ray counts for live-time, geometrical acceptance, efficiencies, and contamination from backscattered particles, as expressed in Equation 3:

$$F = \frac{dN}{dE} \times \frac{(1-\delta)}{GF \times \varepsilon \times T}, \tag{3}$$

where dN is the number of observed events within an energy interval dE. The parameter GF represents the geometrical factor, T denotes the total live-time, ε is the overall detection efficiency, and δ is the fraction of events misidentified in charge due to backscattered particles.

The geometrical factor, $GF = 0.27 \pm 0.01$ m^2 sr, is determined by requiring particles to pass through the active regions of both the top SCD layer and the Bottom Counting Detector(BCD). The live-time, T, is estimated as approximately 228.6 days, after accounting for routine calibration periods and instrument dead time [7]. The charge misidentification fraction, δ, is caused by backscattered particles contaminating the charge measurement. The efficiency term ε includes contributions from several factors:

- **Trigger efficiency:** The fraction of events that satisfied either the high-energy (EHI) or low-energy (ELO) trigger conditions among all events within the geometrical acceptance.
- **Interaction efficiency:** The fraction of triggered events in which the first hadronic interaction occurs above the top CAL layer.
- **Trajectory reconstruction efficiency:** The fraction of events with successfully reconstructed tracks that pass through the top layer of the SCD among the interaction-selected events.
- **Trajectory accuracy:** The fraction of reconstructed events in which the intersection point lies within the charge-scanning area (i.e., the "circle of confusion") on the SCD.
- **Charge-selection efficiency:** The fraction of reconstructed events whose charge falls within the defined proton or helium selection range.
- **SCD active-area efficiency:** The ratio of functioning (stable) channels to the total number of readout channels in the top SCD layer.

3. Results

3.1 Proton and helium spectra

The ISS-CREAM proton spectrum has been measured over the energy range from 1.6 TeV to 655 TeV. Figure 4 presents the proton flux as a function of incident energy. The ISS-CREAM results are compared with those from other experiments, including AMS-02 [10–12], CREAM-I and CREAM-III [6], DAMPE [13], CALET [14], and NUCLEON [15]. All flux values are scaled by $E^{2.5}$.

The ISS-CREAM proton spectrum is fitted using a Smoothly Broken Power Law (SBPL) function, defined by Equation 4:

$$\Phi(E) = \Phi_0 \left(\frac{E}{E_0}\right)^{-\gamma} \left[1 + \left(\frac{E}{E_b}\right)^{\frac{\Delta\gamma}{\beta}}\right]^{-\beta} \quad (\mathrm{m}^2\ \mathrm{sr\ s\ GeV})^{-1} \tag{4}$$

Here, Φ_0 and E_0 represent the normalization constants for flux and energy, respectively. The parameter β controls the smoothness of the transition between two spectral indices: γ below the break energy E_b, and $\gamma + \Delta\gamma$ above E_b.

Multiple SBPL fits were performed by varying the upper limit of the fit energy range, and the resulting fits were compared with a single power-law model to assess statistical significance [7]. The fit result for the range 1.6 TeV to 164 TeV shows a spectral softening at a break energy of $E_b = 9.0 \pm 1.3$ TeV. The fitted spectral indices are $\gamma = 2.57 \pm 0.03$ below the break and $\gamma + \Delta\gamma = 2.82 \pm 0.02$ above it. Further details of the SBPL analysis can be found in G. H. Choi, E. S. Seo et al. 2022 [7].

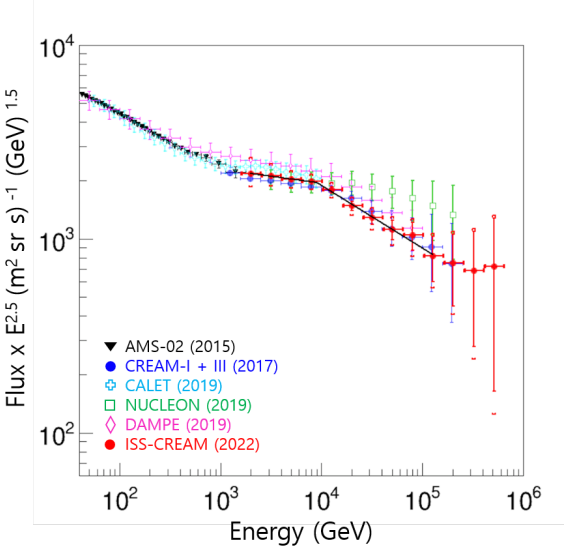

Figure 4: The proton spectrum of the ISS-CREAM experiment is compared with other experiments' data. The statistical uncertainties are represented by error bars, and brackets are obtained by summing the statistical and systematic uncertainties. The SBPL fit result from the energy range of 1.6 – 164 TeV is the black line [7].

Figure 5 presents the proton and preliminary helium spectra measured by the ISS-CREAM experiment as a function of incident energy. The helium spectrum is measured over the energy range from 6 TeV to approximately 1.1 PeV. The preliminary ISS-CREAM helium results are consistent with previous CREAM measurements and extend the energy reach beyond 1 PeV. The spectrum is also compared with results from other experiments, including DAMPE [16] and CALET [17].

The preliminary ISS-CREAM helium flux exceeds the proton flux at around 20 TeV, and the spectral break shows a higher energy than that of the proton. This behavior is consistent with the charge-dependent acceleration limit, $E_{\mathrm{max},Z} = Z \times E_{\mathrm{max},p}$, where $E_{\mathrm{max},p} \sim 50$ TV [18]. The ISS-CREAM helium spectrum will be corrected using improved Monte Carlo simulations to obtain better estimates of efficiency corrections and systematic uncertainties.

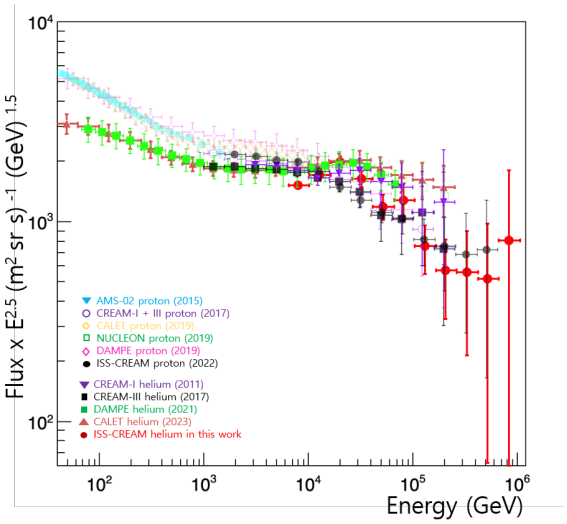

Figure 5: The proton and helium spectra of the ISS-CREAM experiment are compared with other experiments' data. The statistical uncertainties are represented by error bars.

Acknowledgments

This work was supported in the U.S. by NASA grant NNX17AB41G, in Korea by National Research Foundation grants 2022R1F1A1060075 and 2021R1A2B5B03002645, and their predecessor grants, in France by IN2P3/CNRS and CNES, and in Mexico by DGAPA-UNAM project IN109617. The authors thank NASA GSFC WFF and its contractors for engineering support and project management, the JSC ISS Program Office for launch support and ISS accommodation, MSFC for operational support, and KSC and SpaceX for launch support.

References

[1] E. S. Seo et al., Cosmic Ray Energetics And Mass for the International Space Station (ISS-CREAM), ASR, 53, 1451-1455 (2014).

[2] I. H. Park et al., Silicon charge detector for the CREAM experiment, Nucl. Instrum. Methods Phys. Res. A., 570, 286 (2007)

[3] H. S. Ahn et al., The Cosmic Ray Energetics And Mass (CREAM) instrument, Nucl. Instrum. Methods Phys. Res. A, 579, 1034-1053 (2007)

[4] S. C. Kang et al., On-orbit performance of the top and bottom counting detectors for the ISS-CREAM experiment on the international space station, Nucl. Adv. Space Res., 64, 2564-2569 (2019)

[5] Y. Amare et al., The Boronated Scintillator Detector of the ISS-CREAM Experiment, Nucl. Instrum. Methods A, 943, 162413 (2019)

[6] Y. S. Yoon et al., Proton and helium spectra from the CREAM-III flight, ApJ, 839, 5 (2017)

[7] G. H. Choi and E. S. Seo et al., Measurement of High-energy Cosmic-Ray Proton Spectrum from the ISS-CREAM Experiment, ApJ., 940, 107 (2022)

[8] G. H. Choi et al., On-orbit performance of the ISS-CREAM SCD, PoS(ICRC2019)048 (2019)

[9] H. G. Zhang et al., Performance of the ISS-CREAM calorimeter in a calibration beam test, Astropart. Phys., 23 (2021)

[10] M. Aguilar et al., Precision Measurement of the Proton Flux in Primary Cosmic Rays from Rigidity 1 GV to 1.8 TV with the Alpha Magnetic Spectrometer on the International Space Station, Phy. Rev. Lett. 114, 171103 (2015)

[11] M. Aguilar et al., Observation of the Identical Rigidity Dependence of He, C, and O Cosmic Rays at High Rigidities by the Alpha Magnetic Spectrometer on the International Space Station, Phy. Rev. Lett. 117, 251101 (2017)

[12] M. Aguilar et al., Properties of Neon, Magnesium, and Silicon Primary Cosmic Rays Results from the Alpha Magnetic Spectrometer, Phy. Rev. Lett. 124, 211102 (2020)

[13] DAMPE Collaboration, Measurement of the cosmic ray proton spectrum from 40 GeV to 100 TeV with the DAMPE satellite, Science Advances, 5, 9 (2019)

[14] O. Adriani et al., Direct Measurement of the Cosmic-Ray Proton Spectrum from 50 GeV to 10 TeV with the Calorimetric Electron Telescope on the International Space Station, Phy. Rev. Lett. 122, 181102 (2019)

[15] V. Grebenyuk et al., Energy spectra of abundant cosmic-ray nuclei in the NUCLEON experiment, Adv. Space Res., 12, 64 (2019)

[16] Measurement of the cosmic ray helium energy spectrum from 70 GeV to 80 TeV with the DAMPE space mission, Phy. Rev. Lett. 126 (2021), 201102

[17] O. Adriani et al., Direct Measurement of the Cosmic-Ray Helium Spectrum from 40 GeV to 250 TeV with the Calorimetric Electron Telescope on the International Space Station, Phy. Rev. Lett. 130 (2023), 171002

[18] D.P. Scrandis, R. Bowman, E.S. Seo, Investigating Cosmic Ray Elemental Spectra and the Atmospheric Muon Neutrino Flux, Adv. Space Res. 70, 9 (2022)